Nuclear Science and Techniques (2026) 37:126
https://doi.org/10.1007/s41365-026-01945-y

Prediction of $p\bar{\Omega}$ states and femtoscopic study

Ye Yan[1,2] · Qi Huang[1] · Qian Wu[3,4] · Hong-Xia Huang[1] · Jia-Lun Ping[1]

Received: 12 September 2025 / Revised: 10 November 2025 / Accepted: 18 November 2025 / Published online: 16 April 2026

Abstract
Inspired by recent research on the $p\Omega$ and $p\bar{\Lambda}$ systems, we investigate the $p\bar{\Omega}$ systems within the framework of the quark delocalization color-screening model. Our results indicate that the nucleon–$\bar{\Omega}$ interaction is slightly stronger than the nucleon–Ω interaction, implying a higher likelihood of the $p\bar{\Omega}$ system to forming bound states. Dynamic calculations show that the $p\bar{\Omega}$ systems with $J^P = 1^-$ and 2^- form bound states, whose binding energies are deeper than that of the $p\Omega$ system with $J^P = 2^+$. The scattering phase shifts and extracted scattering parameters also support the existence of $p\bar{\Omega}$ bound states. Additionally, we discuss the behavior of the femtoscopic correlation function for $p\bar{\Omega}$ pairs for the first time. Building on the recent experimental progress on the $p\Omega$ correlation function, future femtoscopic investigations of the $p\bar{\Omega}$ system in heavy-ion collisions will be particularly valuable for constraining baryon–antibaryon interactions.

Keywords $p\bar{\Omega}$ systems · Femtoscopic correlation function · Bound states · Hadron–hadron interaction · Scattering phase shifts

1 Introduction

The study of baryon–antibaryon bound states dates back to the proposal by Fermi and Yang [1] to form pions from nucleon–antinucleon pairs. In the traditional one-boson-exchange theory of nucleon–nucleon interactions, it is shown that the nucleon–antinucleon system is more attractive than the nucleon–nucleon system owing to the strong ω-exchange [2]. Therefore, possible bound states and resonances of nucleon–antinucleon systems have been proposed for several years. An extensive and comprehensive review of the possible bound states of $N\bar{N}$ was provided in Ref. [3].

More recently, the BESIII Collaboration reported the observation of a new $X(1880)$ state in the line shape of the $3(\pi^+\pi^-)$ invariant mass spectrum [4], which is considered as evidence for the existence of a proton–antiproton bound state. Many theoretical studies have been conducted to study the $p\bar{p}$ system and the properties of $X(1880)$ [5–11]. In addition to the possible proton–antiproton state, there has also been significant progress in recent studies related to $p\bar{\Lambda}$ [12]. A narrow structure in the $p\bar{\Lambda}$ system near the mass threshold, named $X(2085)$, is observed in the process $e^+e^- \to pK^-\bar{\Lambda}$ with a statistical significance exceeding 20σ. Its spin and parity are slightly favored to be $J^P = 1^+$ based on an amplitude analysis. Further theoretical results and discussions can be found in Refs. [13–15]. Building on the significant progress in studies of nucleon–antinucleon and nucleon–$\bar{\Lambda}$ systems, it is natural to explore whether bound states or resonance states can be formed between nucleons and other hyperons or between nucleons and other antihyperons.

In recent years, progress in understanding the strange dibaryon $p\Omega$ has renewed interest in dibaryon systems. The STAR Collaboration measured the $p\Omega$ correlation functions in Au+Au collisions at the Relativistic Heavy-Ion Collider (RHIC) [16] and reported a positive scattering length for the $p\Omega$ interaction, which supports the hypothesis of a $p\Omega$ bound

This work was supported by the National Natural Science Foundation of China (Nos. 12575088, 12305087, 11535005, and 11675080).

✉ Hong-Xia Huang
hxhuang@njnu.edu.cn

1 Department of Physics, Nanjing Normal University, Nanjing 210023, China

2 Changzhou College of Information Technology, Changzhou 213164, China

3 School of Physics, Nanjing University, Nanjing 210000, China

4 Institute of Modern Physics, Chinese Academy of Sciences, Lanzhou 730000, China

state. In addition, the ALICE Collaboration reported measurements of the p-Ω correlation in pp collisions at $\sqrt{s} = 13$ TeV at the Large Hadron Collider (LHC) [17]. Beyond the $p\Omega$ system, femtoscopic techniques and correlation function studies have made significant progress, both experimentally [18–24] and theoretically [25–57].

The $S = -3$, $I = 1/2$, $J = 2$ $N\Omega$ state was first predicted by J. T. Goldman et al. as a narrow resonance in a relativistic quark model [58]. M. Oka also proposed the existence of a quasi-bound state with $I(J^P) = 1/2(2^+)$ using a constituent quark model [59]. A lattice QCD study by the HAL QCD Collaboration reported that the $p\Omega$ state is a bound state at a pion mass of 875 MeV [60]. Later, the bound nature was also confirmed with nearly physical quark masses ($m_\pi \simeq 146$ MeV and $m_K \simeq 525$ MeV) [61]. Using the interactions obtained from $(2 + 1)$-flavor lattice QCD simulations, K. Morita et al. studied the two-pair momentum correlation functions of the $p\Omega$ state in relativistic heavy-ion collisions to further investigate the existence of a $p\Omega$ bound state [62, 63]. This state has also been confirmed to be a bound state in the frameworks of the chromomagnetic model [64], QCD sum rules [65], and other quark models [66–68]. Additionally, studies on the production of $p\Omega$ and $NN\Omega$ systems can be found in Refs. [69–71].

By analogy to the nucleon–nucleon and nucleon–antinucleon systems, one may expect attractive interactions in both the $p\Omega$ and $p\bar{\Omega}$ channels. If the $p\Omega$ state can be confirmed through further experimental measurements, we expect to observe an even stronger signal for the $p\bar{\Omega}$ state in experiments. Furthermore, the nucleon–antinucleon state would annihilate rapidly in the ground state owing to the quark content of this system, making it challenging to provide a convincing theoretical confirmation of the nucleon–antinucleon bound state or resonance. In contrast, the $p\bar{\Omega}$ state cannot annihilate into the vacuum, as the nucleon consists of three $u(d)$ quarks and $\bar{\Omega}$ consists of three $\bar{s}$ quarks. In this context, the $p\bar{\Omega}$ state is expected to be relatively stable and may serve as an ideal system for studying baryon–antibaryon interactions. The copious production of antibaryons in high-energy colliders offers excellent opportunities to study this type of spectrum. Clearly, the theoretical study of the $p\bar{\Omega}$ system is both interesting and necessary, as it can provide valuable insights for the experimental search for baryon–antibaryon bound states.

In our previous work, we studied the $p\Omega$ interactions and correlation functions based on the quark delocalization color-screening model (QDCSM) [72]. According to our calculations, the depletion of the $p\Omega$ correlation functions caused by the $J^P = 2^+$ bound state, which is not observed in the ALICE Collaboration's measurements [17], can be explained by the contribution of the attractive $J^P = 1^+$ component in spin averaging. The QDCSM is a constituent quark model [73, 74] that introduces two key ingredients: first, quark delocalization, which accounts for orbital excitation by allowing quarks to delocalize from one cluster to another; second, the color-screening factor, which modifies the confinement interaction between quarks in different clusters orbits. In the study of nucleon–nucleon and nucleon–hyperon interactions and the properties of the deuteron, the mechanism of quark delocalization and color screening plays a crucial role in generating intermediate-range attraction [75–77]. This model has also been used to investigate various dibaryon candidates, such as d^* [78], $p\Omega$ [67, 72], and others [79–83]. It has been extended to study baryon–antibaryon systems, including $p\bar{p}$ and $p\bar{\Lambda}$ [84, 85]. Extending it to the $p\bar{\Omega}$ system is a natural progression. Therefore, we continue to investigate the $p\bar{\Omega}$ system within the framework of the QDCSM. In this study, the $p\bar{\Omega}$ system is studied from three aspects: energy spectrum, scattering processes, and correlation functions.

The remainder of this paper is organized as follows. A brief introduction to the QDCSM is provided in the next section. The correlation function and inverse scattering method are introduced in Sects. 2.2 and 2.3, respectively. Section 3 presents to the numerical results and discussion of the study. A summary is presented in the final section.

2 Theoretical formalism

2.1 Quark delocalization color-screening model

The details of the QDCSM employed in the present study can be found in Refs. [73–77]. Here, we present the salient features of this model. The model Hamiltonian is given by

$$
\begin{aligned}
H = & \sum_{i=1}^{6}\left(m_i + \frac{\boldsymbol{p}_i^2}{2m_i}\right) - T_{\mathrm{c.m}} + \sum_{j>i=1}^{3} V_{qq}(\boldsymbol{r}_{ij}) \\
& + \sum_{j>i=4}^{6} V_{\bar{q}\bar{q}}(\boldsymbol{r}_{ij}) + \sum_{i=1}^{3}\sum_{j=4}^{6} V_{q\bar{q}}(\boldsymbol{r}_{ij}),
\end{aligned} \tag{1}
$$

where m_i is the quark mass, $\boldsymbol{p}_i$ is the momentum of the quark, and $T_{\mathrm{c.m.}}$ is the center-of-mass kinetic energy. The dynamics of the hexaquark system are driven by two-body potentials, including color confinement (V_{CON}), perturbative one-gluon exchange interaction (V_{OGE}), and dynamic chiral symmetry breaking (V_χ).

$$
V(\boldsymbol{r}_{ij}) = V_{\mathrm{CON}}(\boldsymbol{r}_{ij}) + V_{\mathrm{OGE}}(\boldsymbol{r}_{ij}) + V_\chi(\boldsymbol{r}_{ij}). \tag{2}
$$

Here, a phenomenological color-screening confinement potential (V_{CON}) is used as follows:

$$
V_{\mathrm{CON}}(\boldsymbol{r}_{ij}) = -a_c \lambda_i^c \cdot \lambda_j^c \left[f(\boldsymbol{r}_{ij}) + V_0\right], \tag{3}
$$

$$f(\boldsymbol{r}_{ij}) = \begin{cases} \boldsymbol{r}_{ij}^2, & i,j \text{ occur in the same cluster} \\ \frac{1-e^{-\mu_{q_iq_j}r_{ij}^2}}{\mu_{q_iq_j}}, & i,j \text{ occur in different cluster} \end{cases}$$

where a_c, V_0 and $\mu_{q_iq_j}$ are model parameters, and λ^c represents the SU(3) color Gell–Mann matrices. Among them, the color-screening parameter $\mu_{q_iq_j}$ is determined by fitting the deuteron properties, nucleon–nucleon scattering phase shifts, and hyperon–nucleon scattering phase shifts, respectively, with $\mu_{qq} = 0.45$, $\mu_{qs} = 0.19$, and $\mu_{ss} = 0.08$ fm^{-2}, satisfying the relation—$\mu_{qs}^2 = \mu_{qq}\mu_{ss}$ [86]. The one-gluon exchange potential (V_{OGE}) is expressed as:

$$V_{\mathrm{OGE}}(\boldsymbol{r}_{ij}) = \frac{1}{4}\alpha_{s_{q_iq_j}}\lambda_i^c\cdot\lambda_j^c \times\left[\frac{1}{r_{ij}}-\frac{\pi}{2}\delta(\mathbf{r}_{ij})\left(\frac{1}{m_i^2}+\frac{1}{m_j^2}+\frac{4\boldsymbol{\sigma}_i\cdot\boldsymbol{\sigma}_j}{3m_im_j}\right)\right], \tag{4}$$

where $\boldsymbol{\sigma}$ is the Pauli matrix and α_s is the quark–gluon coupling constant. To cover the wide energy range from light to strange quarks, an effective scale-dependent quark–gluon coupling $\alpha_s(\mu)$ was introduced [87]:

$$\alpha_s(\mu) = \frac{\alpha_0}{\ln\left(\frac{\mu^2+\mu_0^2}{\Lambda_0^2}\right)}. \tag{5}$$

Owing to the dynamical breaking of chiral symmetry, SU(3) Goldstone boson exchange interactions arise between the constituent light quarks u, d, and s. Accordingly, the chiral interaction is expressed as:

$$V_\chi(\boldsymbol{r}_{ij}) = V_\pi(\boldsymbol{r}_{ij}) + V_K(\boldsymbol{r}_{ij}) + V_\eta(\boldsymbol{r}_{ij}). \tag{6}$$

Among them,

$$V_\pi(\boldsymbol{r}_{ij}) = \frac{g_{\mathrm{ch}}^2}{4\pi}\frac{m_\pi^2}{12m_im_j}\frac{\Lambda_\pi^2}{\Lambda_\pi^2-m_\pi^2}m_\pi\left[Y(m_\pi\boldsymbol{r}_{ij}) -\frac{\Lambda_\pi^3}{m_\pi^3}Y(\Lambda_\pi\boldsymbol{r}_{ij})\right](\boldsymbol{\sigma}_i\cdot\boldsymbol{\sigma}_j)\sum_{a=1}^{3}\left(\lambda_i^a\cdot\lambda_j^a\right), \tag{7}$$

$$V_K(\boldsymbol{r}_{ij}) = \frac{g_{\mathrm{ch}}^2}{4\pi}\frac{m_K^2}{12m_im_j}\frac{\Lambda_K^2}{\Lambda_K^2-m_K^2}m_K\left[Y(m_K\boldsymbol{r}_{ij}) -\frac{\Lambda_K^3}{m_K^3}Y(\Lambda_K\boldsymbol{r}_{ij})\right](\boldsymbol{\sigma}_i\cdot\boldsymbol{\sigma}_j)\sum_{a=4}^{7}\left(\lambda_i^a\cdot\lambda_j^a\right), \tag{8}$$

$$V_\eta(\boldsymbol{r}_{ij}) = \frac{g_{\mathrm{ch}}^2}{4\pi}\frac{m_\eta^2}{12m_im_j}\frac{\Lambda_\eta^2}{\Lambda_\eta^2-m_\eta^2}m_\eta\left[Y(m_\eta\boldsymbol{r}_{ij}) -\frac{\Lambda_\eta^3}{m_\eta^3}Y(\Lambda_\eta\boldsymbol{r}_{ij})\right](\boldsymbol{\sigma}_i\cdot\boldsymbol{\sigma}_j)\left[\cos\theta\left(\lambda_i^8\cdot\lambda_j^8\right) -\sin\theta\left(\lambda_i^0\cdot\lambda_j^0\right)\right], \tag{9}$$

where $Y(x) = e^{-x}/x$ is the standard Yukawa function. The physical η meson is considered by introducing the angle θ instead of the octet one. The λ^a are SU(3) flavor Gell–Mann matrices. The values of m_π, m_k, and m_η are the masses of the SU(3) Goldstone bosons, which adopt the experimental values [88]. The chiral coupling constant g_{ch} is determined from the πNN coupling constant through

$$\frac{g_{\mathrm{ch}}^2}{4\pi} = \left(\frac{3}{5}\right)^2\frac{g_{\pi NN}^2}{4\pi}\frac{m_{u,d}^2}{m_N^2}. \tag{10}$$

Assuming that flavor SU(3) is an exact symmetry, it is only broken by the different masses of the strange quark. The other symbols in the above expressions have their usual definition.

As for $V_{\bar{q}\bar{q}}(\boldsymbol{r}_{ij})$ and $V_{q\bar{q}}(\boldsymbol{r}_{ij})$ in Eq. (1), which represent the antiquark–antiquark ($\bar{q}\bar{q}$) and quark–antiquark ($q\bar{q}$) interactions, for the antiquark, we replace λ_i^c in Eqs. (3) and (4) with $-\lambda_i^{c*}$ and replace λ_i^a in Eqs. (7)–(9) with λ_i^{a*}. In this way, the forms of $V_{\bar{q}\bar{q}}$ and $V_{q\bar{q}}$ can be derived. It is noted that there is no annihilation between the quark and antiquark. This is because the $p\bar{\Omega}$ state cannot annihilate in the vacuum owing to the different quark flavor contents of N and $\bar{\Omega}$. All parameters used in this work and the calculated baryon masses are listed in Tables 1 and 2, respectively. In the quark model, the corresponding antibaryons have the same mass as their baryon partners.

In addition, quark delocalization was introduced to enlarge the model variational space to consider the mutual distortion or internal excitations of nucleons during the interaction. It is realized by specifying the single-particle orbital wave function of the QDCSM as a linear combination

Table 1 Two parameter sets used in this work: $m_\pi = 0.7$, $m_K = 2.51$, $m_\eta = 2.77$, $\Lambda_\pi = 4.2$, $\Lambda_K = 5.2$, $\Lambda_\eta = 5.2$ fm^{-1}, $g_{\mathrm{ch}}^2/(4\pi) = 0.54$

m_q (MeV)	m_s (MeV)	b (fm)	a_c (MeV $\cdot$ fm^{-2})
313 (313)	573 (539)	0.518 (0.6)	58.03 (18.53)
V_0 (MeV)	α_0	Λ_0 (fm^{-1})	μ_0 (MeV)
−1.29 (−0.33)	0.510 (0.709)	1.525 (1.722)	445.81 (445.85)
μ_{qq}	μ_{qs}	μ_{ss}	
0.45(1.2)	0.19(0.30)	0.08 (0.08)	

Table 2 Masses of ground-state baryons (in MeV) with two parameter sets

Baryon	$I(J^P)$	M^{Exp}	M^{Theo}
N	$1/2(1/2^+)$	939	939 (939)
Δ	$3/2(3/2^+)$	1232	1232 (1232)
Λ	$0(1/2^+)$	1116	1124 (1118)
Σ	$1(1/2^+)$	1193	1238 (1224)
Σ^*	$1(3/2^+)$	1385	1360 (1358)
Ξ	$1/2(1/2^+)$	1318	1374 (1365)
Ξ^*	$1/2(3/2^+)$	1533	1496 (1499)
Ω	$0(3/2^+)$	1672	1642 (1654)

of left and right Gaussians, the single-particle orbital wave functions used in the ordinary quark cluster model

$$\begin{aligned}\psi_\alpha(\boldsymbol{S}_i,\epsilon) &= \left(\phi_\alpha(\boldsymbol{S}_i)+\epsilon\phi_\alpha(-\boldsymbol{S}_i)\right)/N(\epsilon),\\ \psi_\beta(-\boldsymbol{S}_i,\epsilon) &= \left(\phi_\beta(-\boldsymbol{S}_i)+\epsilon\phi_\beta(\boldsymbol{S}_i)\right)/N(\epsilon),\\ N(S_i,\epsilon) &= \sqrt{1+\epsilon^2+2\epsilon e^{-S_i^2/4b^2}}.\end{aligned} \tag{11}$$

It is worth noting that the mixing parameter ϵ is not an adjusted parameter but is determined variationally by the dynamics of the multiquark system itself. In this way, the multiquark system chooses its favorable configuration during the interaction process. This mechanism has been used to explain the crossover transition between the hadron phase and quark–gluon plasma phase [89].

2.2 Two-particle correlation function

Experimentally, the correlation function $C(\boldsymbol{k})$ can be measured based on:

$$C(\boldsymbol{k}) = \xi(\boldsymbol{k})\frac{N_{\text{same}}(\boldsymbol{k})}{N_{\text{mixed}}(\boldsymbol{k})}, \tag{12}$$

where $N_{\text{same}}(\boldsymbol{k})$ and $N_{\text{mixed}}(\boldsymbol{k})$ represent the $\boldsymbol{k}$ distributions of hadron–hadron pairs produced in the same and in different collisions, respectively, and $\xi(\boldsymbol{k})$ denotes the corrections for experimental effects. In theoretical studies, the correlation function can be calculated using the Koonin−Pratt (KP) formula [90–92]:

$$\begin{aligned}C(\boldsymbol{k}) &= \frac{N_{12}(\boldsymbol{p}_1,\boldsymbol{p}_2)}{N_1(\boldsymbol{p}_1)N_2(\boldsymbol{p}_2)}\\ &\simeq \frac{\int \mathrm{d}^4x_1\,\mathrm{d}^4x_2 S_1(x_1,\boldsymbol{p}_1)S_2(x_2,\boldsymbol{p}_2)|\Psi(\boldsymbol{r},\boldsymbol{k})|^2}{\int \mathrm{d}^4x_1\,\mathrm{d}^4x_2 S_1(x_1,\boldsymbol{p}_1)S_2(x_2,\boldsymbol{p}_2)}\\ &\simeq \int \mathrm{d}\boldsymbol{r} S_{12}(r)|\Psi(\boldsymbol{r},\boldsymbol{k})|^2,\end{aligned} \tag{13}$$

where $S_i(x_i,\boldsymbol{p}_i)$ $(i=1,2)$ is the single-particle source function of the hadron i with momentum $\boldsymbol{p}_i$, $\boldsymbol{k}=(m_2\boldsymbol{p}_1-m_1\boldsymbol{p}_2)/(m_1+m_2)$ is the relative momentum in the center of mass of the pair $(\boldsymbol{p}_1+\boldsymbol{p}_2=0)$, $\boldsymbol{r}$ is the relative coordinate with time difference correction, and $\Psi(\boldsymbol{r},\boldsymbol{k})$ is the relative wave function in the two-body outgoing state with an asymptotic relative momentum $\boldsymbol{k}$. In the case where we can ignore the time difference of the emission and the momentum dependence of the source, we integrate out the center-of-mass coordinate and obtain Eq. (13), where $S_{12}(r)$ is the normalized pair source function in the relative coordinate, given by the expression:

$$S_{12}(r) = \frac{1}{\left(4\pi R^2\right)^{3/2}}\exp\left(-\frac{r^2}{4R^2}\right), \tag{14}$$

where R is the size parameter of the source. Thus, two important factors of the correlation function are included in Eq. (13): the collision system, which is related to the source function $S_{12}(r)$, and the two-particle interaction, which is embedded in the relative wave function $\Psi(\boldsymbol{r},\boldsymbol{k})$.

For a pair of non-identical particles, such as $p\bar{\Omega}$, assuming that only S-wave part of the wave function is modified by the two-particle interaction, $\Psi(\boldsymbol{r},\boldsymbol{k})$ can be expressed as:

$$\Psi_{p\bar{\Omega}}(\boldsymbol{r},\boldsymbol{k}) = \exp(\mathrm{i}\boldsymbol{k}\cdot\boldsymbol{r}) - j_0(kr) + \psi_{p\bar{\Omega}}(r,k), \tag{15}$$

where the spherical Bessel function $j_0(kr)$ represents the S-wave part of the non-interacting wave function, and $\psi_{p\bar{\Omega}}$ represents the scattering wave function affected by the two-particle interaction. Substituting the relative wave function $\Psi_{p\bar{\Omega}}(\boldsymbol{r},\boldsymbol{k})$ into the KP formula yields the following correlation function:

$$C_{p\bar{\Omega}}(k) = 1 + \int_0^\infty 4\pi r^2\,\mathrm{d}r\,S_{12}(r)\left[|\psi_{p\bar{\Omega}}(r,k)|^2 - |j_0(kr)|^2\right]. \tag{16}$$

$\psi_{p\bar{\Omega}}(r,k)$ can be obtained by solving the Schrödinger equation, and a similar approach has been utilized in the femtoscopic correlation analysis tool using the Schrödinger equation [93]:

$$-\frac{\hbar^2}{2\mu}\nabla^2\psi_{p\bar{\Omega}}(r,k) + V(r)\psi_{p\bar{\Omega}}(r,k) = E\psi_{p\bar{\Omega}}(r,k) \tag{17}$$

where $\mu = m_p m_\Omega/(m_p+m_\Omega)$ is the reduced mass of the system.

Considering the case of the S-wave, the wave function can be separated into a radial term $R_k(r)$ and an angular term $Y_0^0(\theta,\phi)$ and expressed as:

$$\psi_{p\bar{\Omega}}(r,\theta,\phi) = R_k(r)Y_0^0(\theta,\phi). \tag{18}$$

Considering the interaction between a proton and an $\bar{\Omega}$ baryon, which includes both the strong interaction and the repulsive Coulomb interaction, the potential can be written as:

$$V(r) = V_{\mathrm{Strong}}(r) + V_{\mathrm{Coulomb}}(r), \tag{19}$$

where $V_{\mathrm{Coulomb}}(r) = +\alpha\hbar c/r$, and α is the fine-structure constant. The method to obtain the strong interaction potential $V_{\mathrm{Strong}}(r)$ is introduced in the next section.

Once the total interaction potential is determined, the radial Schrödinger equation can be solved as follows:

$$\frac{-\hbar^2}{2\mu}\frac{\mathrm{d}^2 u_k(r)}{\mathrm{d}r^2} + V(r)u_k(r) = Eu_k(r), \tag{20}$$

where $E = \hbar^2k^2/(2\mu)$ and $u_k(r) = rR_k(r)$. On this basis, the correlation function $C_{p\bar{\Omega}}(k)$ for given spin–parity quantum numbers can be calculated using Eq. (16). The calculation of the correlation functions described above is based on obtaining the scattering wave functions by solving the Schrödinger equation in coordinate space [26–28, 30, 32, 33, 36]. Additionally, the scattering wave functions can be obtained by solving the Lippmann–Schwinger (Bethe–Salpeter) equation in momentum space [29, 31, 38, 39]. Further details on the correlation functions for various systems can be found in the references mentioned above.

Additionally, for the S-wave $p\bar{\Omega}$ dibaryon system, the possible spin–parity quantum numbers are $J^P = 1^-$ and 2^-, respectively. Because the experimentally measured correlation function is spin-averaged, the theoretically obtained correlation function should also consider the average over systems with different quantum numbers:

$$C_{p\bar{\Omega}}(k) = \frac{3}{8}C^{J=1}_{p\bar{\Omega}}(k) + \frac{5}{8}C^{J=2}_{p\bar{\Omega}}(k). \tag{21}$$

2.3 Gel'fand–Levitan–Marchenko method for inverse scattering problem

To solve Eq. (20), two-body interaction potential $V(r)$ is absolutely necessary. The QDCSM is a treatment of the few-body problem, which means that directly extracting a two-body interaction potential $V(r)$ from it will not be so natural. Hence, the QDCSM can be employed to investigate the scattering processes, from which the desired potential can be obtained, because hadronization is fully incorporated in the model.

The approach we adopted to extract the two-body equivalent potential $V(r)$ is the GLM method, which is a powerful tool in inverse scattering theory [94]. It can provide a systematic approach to reconstruct an equivalent potential from the scattering data of a specific process, which makes it a very classical "inverse problem". Thus, this method provides another path to understand the nature of two-body interactions.

The key equation of the GLM method used in this study is the Marchenko equation [95, 96], which can be written in the S-wave case in an integration equation form as:

$$K(r,r') + F(r,r') + \int_r^{\infty} K(r,s)F(s,r')\,\mathrm{d}s = 0. \tag{22}$$

Here, the kernel function $K(r,r')$ is the solution of the equation to be determined, and $F(r,r')$ is the inverse Fourier transformation of reflection coefficient as:

$$\begin{aligned} F(r,r') =& \frac{1}{2\pi}\int_{-\infty}^{\infty} e^{\mathrm{i}kr}\{1 - S(k)\}e^{\mathrm{i}kr'}\,\mathrm{d}k \\ &+ \sum_{i=1}^{n} M_i e^{-\kappa_i r}e^{-\kappa_i r'}. \end{aligned} \tag{23}$$

The partial-wave scattering matrix $S(k)$ is given by $S(k) = \exp(2\mathrm{i}\delta(k))$, where $\delta(k)$ is the scattering phase shift satisfying $k\cot\delta = -1/a_0 + 1/2\, r_{\mathrm{eff}}k^2$. Here, a_0 and r_{eff} represent the scattering length and effective range, respectively. Additionally, n is the number of bound states, κ_i denotes the wavenumber of the i-th bound state, and M_i is the norming constant. Then, after solving the Marchenko equation and obtaining $K(r,r')$, the potential can be reconstructed as:

$$V(r) = -2\frac{\mathrm{d}}{\mathrm{d}r}K(r,r). \tag{24}$$

We would like to emphasize one point here. Generally, when bound states exist, this method cannot provide a fully determined potential but ends with a set of phase-equivalent potentials [97]. However, if all the M_i are fixed in a unique way, such as calculating from the Jost solution, the obtained potential will be unique for further calculations [98, 99]. Using this method, further calculations can be performed. For a more comprehensive discussion of this method, please refer to Refs. [94–102].

3 Results and discussion

The S-wave $p\bar{\Omega}$ systems with isospin $I = 1/2$, spin parity $J^P = 1^-$ and 2^- are investigated based on the QDCSM. To determine whether a bound state exists, a dynamic calculation was performed as the first step. The resonating group method (RGM) was employed to solve the bound state problem. In this approach, the total wave function of the six-quark (three quarks and three antiquarks) system is constructed as:

$$\Psi = \mathcal{A}\phi_p(\xi_1)\phi_{\bar{\Omega}}(\xi_2)\chi(\mathbf{R}), \tag{25}$$

where ϕ_p and $\phi_{\bar{\Omega}}$ are the internal wave functions of the proton and $\bar{\Omega}$ clusters, $\chi(\mathbf{R})$ represents the relative motion wave function, and $\mathcal{A}$ is the antisymmetrization operator that accounts for quark exchange effects. The RGM equation is

Table 3 Calculated binding energies (MeV) of the $p\bar{\Omega}$ systems for different spin–parity states with two parameter sets

J^P	$E_{\rm th}^{\rm Theo}$	$E^{\rm Theo}$	$E_{\rm B}$
1^-	2581 (2593)	2571 (2575)	10 (18)
2^-	2581 (2593)	2572 (2577)	9 (16)

derived by projecting the Schrödinger equation onto the cluster basis, leading to a coupled integro-differential equation:

$$\int \left[H(\mathbf{R}, \mathbf{R}') - EN(\mathbf{R}, \mathbf{R}')\right] \chi(\mathbf{R}') \, \mathrm{d}\mathbf{R}' = 0, \tag{26}$$

where H and N are Hamiltonian and normalization kernels, respectively. The relative wave function $\chi(\mathbf{R})$ is expanded using Gaussian basis functions, converting the integral equation into a generalized eigenvalue problem. Solving this equation provides the binding energies and wave functions of the $p\bar{\Omega}$ states. This method has been widely and successfully applied to baryon–baryon interactions and multiquark systems [103–105].

The binding energies of the $p\bar{\Omega}$ systems with $J^P = 1^-$ and $J^P = 2^-$, denoted as $E_{\rm B}$, are listed in Table 3. Here, $E_{\rm th}^{\rm Theo}$ represents the theoretical threshold and $E^{\rm Theo}$ represents the eigenvalue of the corresponding system. The calculation for the $p\bar{\Omega}$ systems does not involve channel coupling because we limit our study to color-singlet sub-clusters consisting of three u/d quarks and three $\bar{s}$ quarks.

From Table 3, we can see that both the $J^P = 1^-$ and $J^P = 2^-$ $p\bar{\Omega}$ form bound states with binding energies of approximately 10 MeV and 9 MeV, respectively. By contrast, in our previous work on the $p\Omega$ systems, the single-channel calculation showed that neither the $J^P = 1^+$ nor $J^P = 2^+$ $p\Omega$ is bound. After channel coupling, only the $p\Omega$ with $J^P = 2^+$ forms a bound state with a binding energy of approximately 6 MeV. According to the results obtained with the second parameter set, the binding energies of the $J^P = 1^-$ and $J^P = 2^-$ $p\bar{\Omega}$ states are approximately 18 MeV and 16 MeV, respectively. The corresponding binding energy of the $p\Omega$ state with $J^P = 2^+$ after channel coupling is approximately 14 MeV. These numerical results indicate that it is more likely for the $p\bar{\Omega}$ system rather than the $p\Omega$ system to form bound states in our calculations. Therefore, considering that the attractive $p\Omega$ interaction is implied in the experimental measurements of $p\Omega$ correlation functions [17], we look forward to the experimental progress on $p\bar{\Omega}$ correlation functions in the future.

To further study the interaction between nucleon and $\bar{\Omega}$, we calculated the scattering phase shifts of the $p\bar{\Omega}$ systems. The calculation is based on the well-developed Kohn–Hulthen–Kato (KHK) variational method, and the details of this method can be found in Refs. [82, 104]. The low-energy scattering phase shifts of the $p\bar{\Omega}$ systems with the two parameter sets are shown in Fig. 1. For the $p\bar{\Omega}$ systems with both $J^P = 1^-$ and $J^P = 2^-$, the scattering phase shifts approach 180° when $E_{\rm c.m.} \to 0$ MeV and rapidly decrease when $E_{\rm c.m.}$ increases, which indicates the existence of a bound state in these systems. This conclusion is consistent with the bound state calculation discussed earlier. Then, we can extract the scattering length a_0 and the effective range $r_{\rm eff}$ of the $p\bar{\Omega}$ systems from the low-energy phase shifts obtained above using the expansion:

$$k \cot \delta = -\frac{1}{a_0} + \frac{1}{2} r_{\rm eff} k^2 + \mathcal{O}(k^4), \tag{27}$$

where k is the momentum of the relative motion with $k = \sqrt{2\mu E_{\rm c.m.}}$, μ is the reduced mass of the two baryons, and $E_{\rm c.m.}$ is the incident energy; δ is the low-energy scattering phase shift. The binding energy $E_{\rm B}'$ can be calculated using the following relation:

$$E_{\rm B}' = \frac{\hbar^2 \alpha^2}{2\mu}, \tag{28}$$

where α is the wave number, which can be obtained from the relation [106]:

$$r_{\rm eff} = \frac{2}{\alpha}\left(1 - \frac{1}{\alpha a_0}\right). \tag{29}$$

Note that this is another way to calculate the binding energy; therefore, it is labeled $E_{\rm B}'$. The scattering parameters of the $p\bar{\Omega}$ systems, along with the binding energies obtained using the scattering parameters, are presented in Table 4.

From Table 4, our results show that the scattering lengths are positive for the $p\bar{\Omega}$ systems with $J^P = 1^-$ and 2^-, which also confirms the existence of bound states. In addition, the

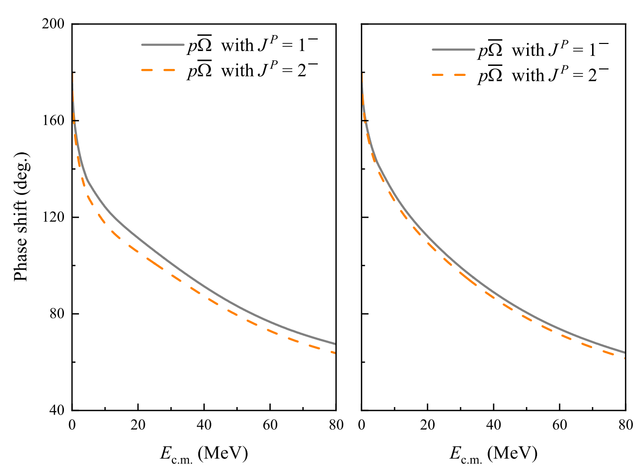

Fig. 1 (Color online) Calculated phase shifts of the $p\bar{\Omega}$ systems for $J^P = 1^-$ and 2^- with two parameter sets

Table 4 Extracted scattering length a_0, effective range r_{eff}, and binding energy E'_{B} of the $p\bar{\Omega}$ systems with two parameter sets

J^P	a_0 (fm)	r_{eff} (fm)	E'_{B} (MeV)
1^-	2.43 (2.02)	0.48 (0.50)	7 (11)
2^-	2.79 (2.10)	0.81 (0.61)	6 (11)

binding energies of the two systems obtained using Eq. (28) are broadly consistent with the numerical results shown in Table 3, which were obtained by dynamic calculation. Additionally, in the method of obtaining the binding energies using scattering parameters, the binding energies of the two $p\bar{\Omega}$ systems are also deeper than that of the $p\Omega$ system with $J^P = 2^+$.

Moreover, by solving the inverse scattering problem, we can further study the behavior of the $p\bar{\Omega}$ correlation functions based on the $p\bar{\Omega}$ scattering process and the KP formula in Eq. (13). Before that, we can study the general properties of the $p\bar{\Omega}$ correlation functions through an effective square well potential model. The correlation functions corresponding to different degrees of the square well potentials are presented in Fig. 2. The solid red lines represent the correlation functions influenced only by the repulsive Coulomb interaction. The dashed blue lines represent the correlation functions influenced only by the square well potentials. We introduce three square well potentials with a width $r_0 = 2$ fm: a weak attraction in panel (a) corresponding to $V_0 = -10$ MeV, a moderate attraction in panel (b) corresponding to $V_0 = -28$ MeV, and a relatively strong attraction in panel (c) corresponding to $V_0 = -40$ MeV. The dotted black lines represent the correlation functions influenced by both the Coulomb interaction and square well potentials through Eq. (19). Additionally, we adopt a source size parameter $R = 0.95$ fm in Eq. (14), which is the same value used in our previous $p\Omega$ correlation analysis [72]. This value was originally extracted by the ALICE Collaboration [17, 107]. It should be emphasized that the source size is determined by the specific collision system and experimental conditions in heavy-ion collisions.

In Fig. 2, panels (a) and (b), the correlation function affected only by the square potential is above unity in the low-energy region, which is due to the attractive interaction. The difference is that the weak attraction is not sufficient to form a bound state; therefore, the correlation function is always above unity, whereas the moderate attraction forms a shallow bound state. The existence of a bound state leads to the depletion of the correlation function; therefore, there exists a part below unity. After considering both the Coulomb interaction and square well potentials, which mainly dominate the low-energy region (0 MeV$< k <$25 MeV), the correlation function forms a peak-like structure. In panel (c), the correlation function remains below unity for a relatively strong attraction. A discussion of this phenomenon can be found in Refs. [39, 72]. After considering the Coulomb interaction, one can see that the correlation function in the low-energy region nearly coincides with the result obtained by considering only the Coulomb interaction. As the relative momentum k increases, the correlation function closely matches the result obtained by considering only a relatively strong attraction between the particles.

After replacing the square well potentials with the effective potentials obtained by solving the inverse scattering problem using the GLM method, which is briefly introduced in Sect. 2.3, we can study the correlation function of the $p\bar{\Omega}$ system. Because the two parameter sets yielded similar results, the discussion of the correlation function is presented based on the first parameter set for conciseness. Both the effective potentials of the $p\bar{\Omega}$ systems with $J^P = 1^-$ and 2^- are obtained. The total $p\bar{\Omega}$ correlation function is a

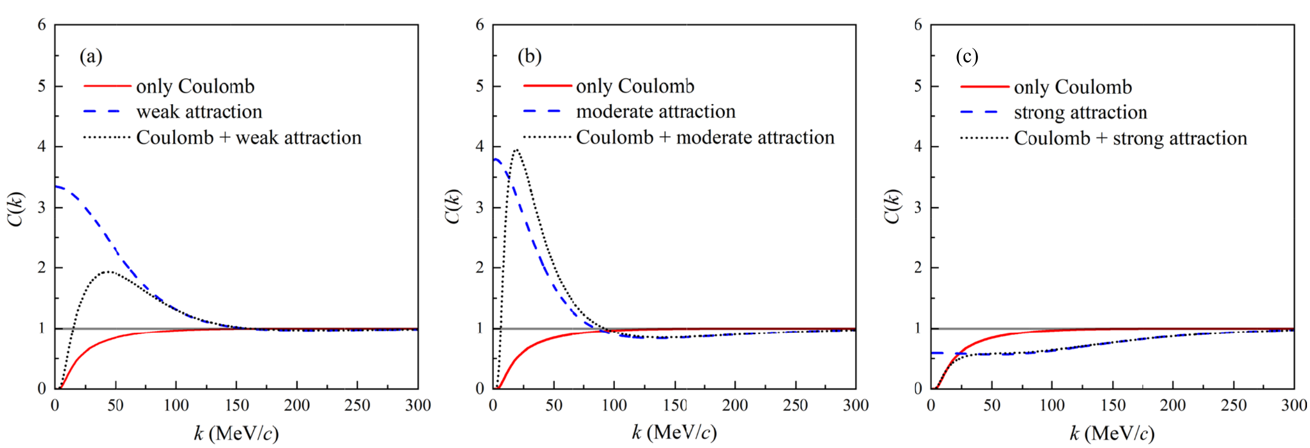

Fig. 2 (Color online) Correlation functions for different square well potentials, with $V(r) = V_0\,\theta(r_0 - r)$, where $V_0 = -10$ MeV in panel (**a**), $V_0 = -28$ MeV in panel (**b**), $V_0 = -40$ MeV in panel (**c**), and $r_0 = 2$ fm

superposition of the correlation functions corresponding to the two quantum numbers according to Eq. (21). Because the $p\bar{\Omega}$ system forms bound states for both quantum numbers and the interactions are similar, we omit the comparison of the correlation functions for the two quantum numbers here. The total correlation functions calculated for different values of the source size parameter R are shown in Fig. 3. In addition, recent studies on emission source properties can be found in Refs. [107–111].

In Fig. 3, panels (a)–(e), the dashed gray lines and the dotted orange lines represent the $p\bar{\Omega}$ correlation functions considering only the Coulomb interaction and both the Coulomb interaction and strong interaction, respectively. In panel (f), the gray band represents the correlation functions influenced only by the Coulomb interaction with the size parameter R ranging from 1.0 to 2.5 fm, while the other lines summarize the correlation functions shown in panels (a)–(e). According to our results, the change in the size parameter R can greatly influence the $p\bar{\Omega}$ correlation functions. An obvious feature is that as R increases, the peak-like structure caused by the different dominant regions of the Coulomb interaction and $p\bar{\Omega}$ strong interaction gradually becomes less obvious and eventually disappears. Because two bound states are obtained in our calculation, it is very important to verify this conclusion using correlation functions. It can be seen that as the correlation function influenced only by the Coulomb interaction gradually approaches unity, the depletion caused by the bound states leads to the correlation function being below that of the Coulomb-only case.

While femtoscopic measurements in heavy-ion collisions provide important access to the $p\bar{\Omega}$ interaction, such bound states may also be produced in other high-energy environments capable of forming multi-strange baryon–antibaryon pairs, such as pp and e^+e^- collisions, as well as high-energy fixed-target experiments, although the production probability may vary across systems. If a $p\bar{\Omega}$ bound state is formed, it can decay through the weak decay of the $\bar{\Omega}$, leading to final states such as $p\bar{\Omega} \to p\bar{\Lambda}K$ and $p\bar{\Omega} \to p\bar{\Xi}\pi$, or through quark rearrangement into a three-meson final state, $p\bar{\Omega} \to KKK$, which may provide complementary detection signatures beyond femtoscopy in future searches.

In recent years, experimental data on correlation functions have increased rapidly [18–24], providing unprecedented insights into hadron–hadron interactions across a variety of systems. Together with femtoscopic techniques, these studies open up new possibilities for extracting low-energy scattering parameters that are otherwise difficult to access. On the theoretical side, continuous progress in lattice QCD, effective field theory, and quark-model-based approaches has greatly enriched our understanding and

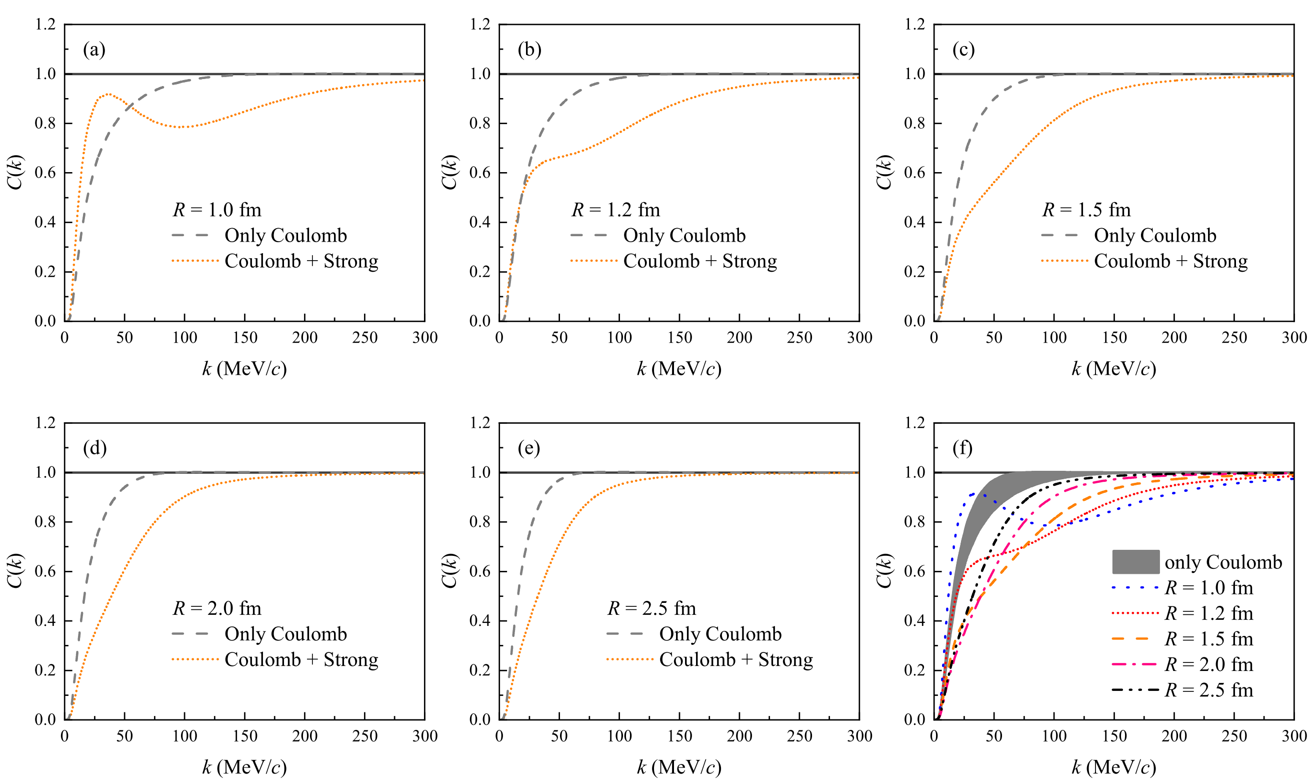

Fig. 3 (Color online) $p\bar{\Omega}$ correlation functions with different values of source size parameter R, where R = 1.0 fm in panel (**a**), R = 1.2 fm in panel (**b**), R = 1.5 fm in panel (**c**), R = 2.0 fm in panel (**d**), and R = 2.5 fm in panel (**e**) are summarized in panel (f)

offered valuable guidance for interpreting the experimental observations [25–57]. The synergy between experimental measurements and theoretical developments will not only deepen our knowledge of strong interactions, but also pave the way for future explorations of exotic hadronic states and nuclear physics [112–114]. In this context, it is well established that nucleon–nucleon and hyperon–nucleon interactions provide the basis for the formation of nuclei and hypernuclei [115–121], while antihyperon–antinucleon interactions give rise to antihypernuclei [122, 123]. An open question is whether antihyperon–nucleon interactions can also give rise to the formation of novel nuclear systems. As a continuation of the present study, we will further explore such systems based on the antihyperon–nucleon interactions obtained in this study.

4 Summary

In this study, we investigate the S-wave $p\bar{\Omega}$ systems with isospin $I = 1/2$, spin parity $J^P = 1^-$ and 2^- in the framework of the QDCSM. The results show that the $p\bar{\Omega}$ systems with both $J^P = 1^-$ and 2^+ form bound states, and the attraction between nucleon and $\bar{\Omega}$ is slightly stronger than that between nucleon and Ω, suggesting that the $p\bar{\Omega}$ system has a higher likelihood of forming bound states than the $p\Omega$ system. The calculation of the low-energy scattering phase shifts and scattering parameters of the $p\bar{\Omega}$ systems also supports the existence of $p\bar{\Omega}$ bound states with $J^P = 1^-$ and 2^-. In addition, considering that a nucleon is composed of three light quarks $u(d)$ and $\bar{\Omega}$ of three strange quarks $\bar{s}$, the $p\bar{\Omega}$ state cannot annihilate into the vacuum. In this context, the $p\bar{\Omega}$ state is a special state that can provide useful information for the experimental search for baryon–antibaryon bound states.

By using the GLM method, we solve the inverse scattering problem and obtain the effective $p\bar{\Omega}$ potentials. On this basis, the $p\bar{\Omega}$ correlation functions are calculated, considering both the Coulomb interaction and spin averaging. We present correlation functions corresponding to different source size parameters R, which can be used for future comparisons with experimental measurements.

Understanding hadron–hadron interactions is an important issue in the study of hadron physics. The study of the interaction between baryons and antibaryons in this work is also an effective method for testing this mechanism. The femtoscopic correlation function has become an important method for exploring hadron–hadron interactions, and further theoretical and experimental investigations are essential for a deeper understanding of such baryon–antibaryon systems.

Author Contributions All authors contributed to the study conception and design. Material preparation, data collection, and analysis were performed by Ye Yan, Qi Huang, Qian Wu, and Hong-Xia Huang. Hong-Xia Huang and Jia-Lun Ping were responsible for review and editing, supervision, project administration, and funding acquisition. The first draft of the manuscript was written by Ye Yan, and all authors commented on previous versions of the manuscript. All authors read and approved the final manuscript.

Data Availability The data that support the findings of this study are openly available in Science Data Bank at https://cstr.cn/31253.11.sciencedb.j00186.00988 and https://www.doi.org/10.57760/sciencedb.j00186.00988.

Declarations

Conflict of interest The authors declare that they have no conflict of interest.

References

1. E. Fermi, C.N. Yang, Are mesons elementary particles? Phys. Rev. **76**, 1739 (1949). https://doi.org/10.1103/PhysRev.76.1739
2. K. Erkelenz, Current status of the relativistic two nucleon one boson exchange potential. Phys. Rept. **13**, 191 (1974). https://doi.org/10.1016/0370-1573(74)90008-8
3. J.M. Richard, Quasinuclear and quark model baryonium: historical survey. Nucl. Phys. B Proc. Suppl. **86**, 361 (2000). https://doi.org/10.1016/S0920-5632(00)00587-9
4. M. Ablikim et al., [BESIII], Observation of the anomalous shape of $X(1840)$ in $J/\psi \to \gamma 3(\pi^+\pi^-)$ indicating a second resonance near $p\bar{p}$ threshold. Phys. Rev. Lett. **132**, 151901 (2024). https://doi.org/10.1103/PhysRevLett.132.151901
5. S.G. Salnikov, A.I. Milstein, Meson production in J/ψ decays and $J/\psi \to N\bar{N}\gamma$ process. Nucl. Phys. B **1002**, 116539 (2024). https://doi.org/10.1016/j.nuclphysb.2024.116539
6. Y. Xiao, J.X. Lu, L.S. Geng, Reexamination of antinucleon-nucleon interactions in covariant chiral effective field theory. Phys. Rev. C **110**, 6 (2024). https://doi.org/10.1103/PhysRevC.110.064002
7. M. Karliner, J.L. Rosner, Possible mixing of a diquark-antidiquark with a $p\bar{p}$ hadronic molecule. Phys. Rev. D **110**, 094058 (2024). https://doi.org/10.1103/PhysRevD.110.094058
8. P.Y. Niu, Z.Y. Zhang, Y.Y. Li et al., Pole structures of the $X(1840)$ or $X(1835)$ and the $X(1880)$. Phys. Rev. D **110**, 094020 (2024). https://doi.org/10.1103/PhysRevD.110.094020
9. P.G. Ortega, D.R. Entem, F. Fernandez et al., Revisiting the proton-antiproton scattering using a constituent-quark-model based coupled-channels calculation. Phys. Lett. B **862**, 139281 (2025). https://doi.org/10.1016/j.physletb.2025.139281
10. Z.S. Jia, Z.H. Zhang, F.K. Guo et al., Coupled-channel analysis of the near-threshold $e^+e^- \to N\bar{N}$ cross sections. Phys. Rev. D **111**, 054014 (2025). https://doi.org/10.1103/PhysRevD.111.054014
11. Q.H. Yang, L.Y. Dai, U.G. Meißner, Quantum numbers of the $X(1880)$. Phys. Rev. D **113**, L011501 (2026). https://doi.org/10.1103/gmyw-cfjf
12. M. Ablikim et al. [BESIII], Determination of spin-parity quantum numbers for the narrow structure near the $p\bar{\Lambda}$ Threshold in $e^+e^- \to pK^-\bar{\Lambda} + c.c.$. Phys. Rev. Lett. **131**, 151901 (2023). https://doi.org/10.1103/PhysRevLett.131.151901
13. T.G. Li, S.C. Zhang, G.Y. Wang et al., Canonical interpretation of the newly observed $J^P = 1^+$ structure $X(2085)$. Phys. Rev.

D **110**, 114020 (2024). https://doi.org/10.1103/PhysRevD.110.114020
14. J. Haidenbauer, U.G. Meißner, $p\bar{\Lambda}$ final-state interaction in the reactions $e^+e^- \to K^-p\bar{\Lambda}$ and $J/\psi \to K^-p\bar{\Lambda}$. Eur. Phys. J. A **60**, 119 (2024). https://doi.org/10.1140/epja/s10050-024-01345-z
15. X.H. Zhang, S.Q. Zhang, C.F. Qiao, The spectra of $p\bar{\Lambda}$ and $p\bar{\Sigma}$ hexaquark states. Eur. Phys. J. C **85**, 693 (2025). https://doi.org/10.1140/epjc/s10052-025-14356-x
16. J. Adam et al., [STAR], The Proton-Ω correlation function in Au + Au collisions at $\sqrt{s_{\mathrm{NN}}} = 200$ GeV. Phys. Lett. B **790**, 490 (2019). https://doi.org/10.1016/j.physletb.2019.01.055
17. ALICE Collaboration, Unveiling the strong interaction among hadrons at the LHC. Nature **588**, 232 (2020) [erratum: Nature **590**, E13 (2021)]. https://doi.org/10.1038/s41586-020-3001-6
18. STAR Collaboration, Measurement of Interaction between Antiprotons. Nature **527**, 345 (2015). https://doi.org/10.1038/nature15724
19. S. Acharya, D. Adamová, S.P. Adhya et al., Scattering studies with low-energy kaon-proton femtoscopy in proton-proton collisions at the LHC. Phys. Rev. Lett. **124**, 092301 (2020). https://doi.org/10.1103/PhysRevLett.124.092301
20. L. Fabbietti, V. Mantovani Sarti, O. Vazquez Doce, Study of the strong interaction among hadrons with correlations at the LHC. Ann. Rev. Nucl. Part. Sci. **71**, 377 (2021). https://doi.org/10.1146/annurev-nucl-102419-034438
21. S. Acharya et al., [ALICE], Experimental Evidence for an Attractive $p-\phi$ Interaction. Phys. Rev. Lett. **127**, 172301 (2021). https://doi.org/10.1103/PhysRevLett.127.172301
22. S. Acharya et al., [ALICE], Exploring the $N\Lambda$-$N\Sigma$ coupled system with high precision correlation techniques at the LHC. Phys. Lett. B **833**, 137272 (2022). https://doi.org/10.1016/j.physletb.2022.137272
23. S. Acharya et al., [ALICE], First study of the two-body scattering involving charm hadrons. Phys. Rev. D **106**, 052010 (2022). https://doi.org/10.1103/PhysRevD.106.052010
24. B.E. Aboona et al., [STAR], Light nuclei femtoscopy and baryon interactions in 3 GeV Au + Au collisions at RHIC. Phys. Lett. B **864**, 139412 (2025). https://doi.org/10.1016/j.physletb.2025.139412
25. A. Ohnishi, Y. Hirata, Y. Nara et al., Can we extract Lambda–Lambda interaction from two particle momentum correlation? Nucl. Phys. A **670**, 297 (2000). https://doi.org/10.1016/S0375-9474(00)00117-2
26. K. Morita, T. Furumoto, A. Ohnishi, ΛΛ interaction from relativistic heavy-ion collisions. Phys. Rev. C **91**, 024916 (2015). https://doi.org/10.1103/PhysRevC.91.024916
27. A. Ohnishi, K. Morita, K. Miyahara et al., Hadron-hadron correlation and interaction from heavy-ion collisions. Nucl. Phys. A **954**, 294 (2016). https://doi.org/10.1016/j.nuclphysa.2016.05.010
28. T. Hatsuda, K. Morita, A. Ohnishi et al., $p\Xi^-$ Correlation in relativistic heavy ion collisions with nucleon-hyperon interaction from lattice QCD. Nucl. Phys. A **967**, 856 (2017). https://doi.org/10.1016/j.nuclphysa.2017.04.041
29. J. Haidenbauer, Coupled-channel effects in hadron-hadron correlation functions. Nucl. Phys. A **981**, 1 (2019). https://doi.org/10.1016/j.nuclphysa.2018.10.090
30. Y. Kamiya, T. Hyodo, K. Morita et al., K^-p Correlation function from high-energy nuclear collisions and chiral SU(3) dynamics. Phys. Rev. Lett. **124**, 132501 (2020). https://doi.org/10.1103/PhysRevLett.124.132501
31. J. Haidenbauer, G. Krein, T.C. Peixoto, Femtoscopic correlations and the Λ_cN interaction. Eur. Phys. J. A **56**, 184 (2020). https://doi.org/10.1140/epja/s10050-020-00190-0
32. A. Ohnishi, Y. Kamiya, K. Sasaki et al., Femtoscopic study of $N\Xi$ interaction and search for the H dibaryon state around the $N\Xi$ threshold. Few Body Syst. **62**, 42 (2021). https://doi.org/10.1007/s00601-021-01626-z
33. K. Ogata, T. Fukui, Y. Kamiya et al., Effect of deuteron breakup on the deuteron-Ξ correlation function. Phys. Rev. C **103**, 065205 (2021). https://doi.org/10.1103/PhysRevC.103.065205
34. S. Mrówczyński, P. Słoń, Deuteron-deuteron correlation function in nucleus-nucleus collisions. Phys. Rev. C **104**, 024909 (2021). https://doi.org/10.1103/PhysRevC.104.024909
35. ŁK. Graczykowski, M.A. Janik, Unfolding the effects of final-state interactions and quantum statistics in two-particle angular correlations. Phys. Rev. C **104**, 054909 (2021). https://doi.org/10.1103/PhysRevC.104.054909
36. Y. Kamiya, K. Sasaki, T. Fukui et al., Femtoscopic study of coupled-channels $N\Xi$ and ΛΛ interactions. Phys. Rev. C **105**, 014915 (2022). https://doi.org/10.1103/PhysRevC.105.014915
37. J. Haidenbauer, U.G. Meißner, Exploring the Σ^+p interaction by measurements of the correlation function. Phys. Lett. B **829**, 137074 (2022). https://doi.org/10.1016/j.physletb.2022.137074
38. Z.W. Liu, K.W. Li, L.S. Geng, Strangeness S = −2 baryon-baryon interactions and femtoscopic correlation functions in covariant chiral effective field theory. Chin. Phys. C **47**, 024108 (2023). https://doi.org/10.1088/1674-1137/ac988a
39. Z.W. Liu, J.X. Lu, L.S. Geng, Study of the DK interaction with femtoscopic correlation functions. Phys. Rev. D **107**, 074019 (2023). https://doi.org/10.1103/PhysRevD.107.074019
40. Z.W. Liu, J.X. Lu, M.Z. Liu et al., Distinguishing the spins of $P_c(4440)$ and $P_c(4457)$ with femtoscopic correlation functions. Phys. Rev. D **108**, L031503 (2023). https://doi.org/10.1103/PhysRevD.108.L031503
41. R. Molina, Z.W. Liu, L.S. Geng et al., Correlation function for the $a_0(980)$. Eur. Phys. J. C **84**, 328 (2024). https://doi.org/10.1140/epjc/s10052-024-12694-w
42. I. Vidana, A. Feijoo, M. Albaladejo et al., Femtoscopic correlation function for the $T_{cc}(3875)^+$ state. Phys. Lett. B **846**, 138201 (2023). https://doi.org/10.1016/j.physletb.2023.138201
43. V.M. Sarti, A. Feijoo, I. Vidaña et al., Constraining the low-energy $S = -2$ meson-baryon interaction with two-particle correlations. Phys. Rev. D **110**, L011505 (2024). https://doi.org/10.1103/PhysRevD.110.L011505
44. R. Molina, C.W. Xiao, W.H. Liang et al., Correlation functions for the $N^*(1535)$ and the inverse problem. Phys. Rev. D **109**, 054002 (2024). https://doi.org/10.1103/PhysRevD.109.054002
45. M. Albaladejo, A. Feijoo, I. Vidaña et al., Inverse problem in femtoscopic correlation functions: the $T_{cc}(3875)^+$ state. Eur. Phys. J. A **61**, 187 (2025). https://doi.org/10.1140/epja/s10050-025-01650-1
46. A. Feijoo, L.R. Dai, L.M. Abreu et al., Correlation function for the T_{bb} state: determination of the binding, scattering lengths, effective ranges, and molecular probabilities. Phys. Rev. D **109**, 016014 (2024). https://doi.org/10.1103/PhysRevD.109.016014
47. H.P. Li, J.Y. Yi, C.W. Xiao et al., Correlation function and the inverse problem in the BD interaction. Chin. Phys. C **48**, 053107 (2024). https://doi.org/10.1088/1674-1137/ad2dc2
48. A. Feijoo, M. Korwieser, L. Fabbietti, Relevance of the coupled channels in the ϕp and $\rho^0 p$ correlation functions. Phys. Rev. D **111**, 014009 (2025). https://doi.org/10.1103/PhysRevD.111.014009
49. N. Ikeno, G. Toledo, E. Oset, Model independent analysis of femtoscopic correlation functions: an application to the $D^*_{s0}(2317)$. Phys. Lett. B **847**, 138281 (2023). https://doi.org/10.1016/j.physletb.2023.138281
50. M. Albaladejo, J. Nieves, E. Ruiz-Arriola, Femtoscopic signatures of the lightest S-wave scalar open-charm mesons. Phys. Rev. D **108**, 014020 (2023). https://doi.org/10.1103/PhysRevD.108.014020

51. J.M. Torres-Rincon, À. Ramos, L. Tolos, Femtoscopy of D mesons and light mesons upon unitarized effective field theories. Phys. Rev. D **108**, 096008 (2023). https://doi.org/10.1103/PhysRevD.108.096008
52. L.M. Abreu, P. Gubler, K.P. Khemchandani et al., A study of the ϕN correlation function. Phys. Lett. B **860**, 139175 (2025). https://doi.org/10.1016/j.physletb.2024.139175
53. H.P. Li, C.W. Xiao, W.H. Liang et al., How to unravel the nature of the $\Sigma^*(1430)(1/2^-)$ state from correlation functions. Phys. Rev. D **110**, 114018 (2024). https://doi.org/10.1103/PhysRevD.110.114018
54. M. Albaladejo, A. Feijoo, J. Nieves et al., Femtoscopy correlation functions and mass distributions from production experiments. Phys. Rev. D **110**, 114052 (2024). https://doi.org/10.1103/PhysRevD.110.114052
55. F. Etminan, Femtoscopic study of the $\Omega\alpha$ interaction in heavy-ion collisions. Phys. Rev. C **111**, 014912 (2025). https://doi.org/10.1103/PhysRevC.111.014912
56. A. Jinno, Y. Kamiya, T. Hyodo et al., Theoretical study on $\Lambda\alpha$ and $\Xi\alpha$ correlation functions. J. Subatomic Part. Cosmol. **1**, 100005 (2024). https://doi.org/10.1016/j.jspc.2024.100005
57. F. Etminan, Exploring the $\phi-\alpha$ interaction via femtoscopic study. Phys. Lett. B **866**, 139564 (2025). https://doi.org/10.1016/j.physletb.2025.139564
58. J.T. Goldman, K. Maltman, G.J. Stephenson et al., Strangeness −3 dibaryons. Phys. Rev. Lett. **59**, 627 (1987). https://doi.org/10.1103/PhysRevLett.59.627
59. M. Oka, Flavor octet dibaryons in the quark model. Phys. Rev. D **38**, 298 (1988). https://doi.org/10.1103/PhysRevD.38.298
60. F. Etminan et al., [HAL QCD], Spin-2 $N\Omega$ dibaryon from Lattice QCD. Nucl. Phys. A **928**, 89 (2014). https://doi.org/10.1016/j.nuclphysa.2014.05.014
61. T. Iritani et al., [HAL QCD], $N\Omega$ dibaryon from lattice QCD near the physical point. Phys. Lett. B **792**, 284 (2019). https://doi.org/10.1016/j.physletb.2019.03.050
62. K. Morita, A. Ohnishi, F. Etminan et al., Probing multistrange dibaryons with proton–omega correlations in high–energy heavy ion collisions. Phys. Rev. C **94**, 031901 (2016) [erratum: Phys. Rev. C **100**, 069902 (2019)]. https://doi.org/10.1103/PhysRevC.94.031901
63. K. Morita, S. Gongyo, T. Hatsuda et al., Probing $\Omega\Omega$ and $p\Omega$ dibaryons with femtoscopic correlations in relativistic heavy-ion collisions. Phys. Rev. C **101**, 015201 (2020). https://doi.org/10.1103/PhysRevC.101.015201
64. B. Silvestre- Brac and J. Leandri, Systematics of q–6 systems in a simple chromomagnetic model. Phys. Rev. D **45**, 4221 (1992). https://doi.org/10.1103/PhysRevD.45.4221
65. X.H. Chen, Q.N. Wang, W. Chen et al., Mass spectra of $N\Omega$ dibaryons in the $^3S_1$ and $^5S_2$ channels. Phys. Rev. D **103**, 094011 (2021). https://doi.org/10.1103/PhysRevD.103.094011
66. L.R. Dai, D. Zhang, C.R. Li et al., Structures of N Omega and Delta Omega dibaryons. Chin. Phys. Lett. **24**, 389 (2007). https://doi.org/10.1088/0256-307X/24/2/024
67. H. Huang, J. Ping, F. Wang, Further study of the $N\Omega$ dibaryon within constituent quark models. Phys. Rev. C **92**, 065202 (2015). https://doi.org/10.1103/PhysRevC.92.065202
68. Q.B. Li, P.N. Shen, N omega and delta omega dibaryons in SU(3) chiral quark model. Eur. Phys. J. A **8**, 417 (2000). https://doi.org/10.1007/s100530050052
69. S. Zhang, Y.G. Ma, Ω-dibaryon production with hadron interaction potential from the lattice QCD in relativistic heavy-ion collisions. Phys. Lett. B **811**, 135867 (2020). https://doi.org/10.1016/j.physletb.2020.135867
70. J. Pu, K.J. Sun, C.W. Ma et al., Probing the internal structures of $p\Omega$ and $\Omega\Omega$ with their production at the Large Hadron Collider. Phys. Rev. C **110**, 024908 (2024). https://doi.org/10.1103/PhysRevC.110.024908
71. L. Zhang, S. Zhang, Y.G. Ma, Production of ΩNN and $\Omega\Omega N$ in ultra-relativistic heavy-ion collisions. Eur. Phys. J. C **82**, 416 (2022). https://doi.org/10.1140/epjc/s10052-022-10336-7
72. Y. Yan, Q. Huang, Y. Yang et al., Investigating the p-Ω interactions and correlation functions. Sci. China Phys. Mech. Astron. **68**, 232012 (2025). https://doi.org/10.1007/s11433-024-2580-9
73. F. Wang, G.H. Wu, L.J. Teng et al., Quark delocalization, color screening, and nuclear intermediate range attraction. Phys. Rev. Lett. **69**, 2901 (1992). https://doi.org/10.1103/PhysRevLett.69.2901
74. G.H. Wu, L.J. Teng, J.L. Ping et al., Quark delocalization, color screening, and NN intermediate range attraction: P waves. Phys. Rev. C **53**, 1161 (1996). https://doi.org/10.1103/PhysRevC.53.1161
75. J.L. Ping, F. Wang, J.T. Goldman, Effective baryon baryon potentials in the quark delocalization and color screening model. Nucl. Phys. A **657**, 95 (1999). https://doi.org/10.1016/S0375-9474(99)00321-8
76. G.H. Wu, J.L. Ping, L.J. Teng et al., Quark delocalization, color screening model and nucleon baryon scattering. Nucl. Phys. A **673**, 279 (2000). https://doi.org/10.1016/S0375-9474(00)00141-X
77. H.R. Pang, J.L. Ping, F. Wang et al., Phenomenological study of hadron interaction models. Phys. Rev. C **65**, 014003 (2002). https://doi.org/10.1103/PhysRevC.65.014003
78. J.L. Ping, H.X. Huang, H.R. Pang et al., Quark models of dibaryon resonances in nucleon-nucleon scattering. Phys. Rev. C **79**, 024001 (2009). https://doi.org/10.1103/PhysRevC.79.024001
79. Y. Yan, Y. Wu, X. Hu et al., Fully heavy pentaquarks in quark models. Phys. Rev. D **105**, 014027 (2022). https://doi.org/10.1103/PhysRevD.105.014027
80. Y. Yan, X. Hu, Y. Wu et al., Pentaquark interpretation of Λ_c states in the quark model. Eur. Phys. J. C **83**, 524 (2023). https://doi.org/10.1140/epjc/s10052-023-11709-2
81. Y. Yan, Y. Wu, H. Huang et al., Prediction of charmed-bottom pentaquarks in quark model. Eur. Phys. J. C **83**, 610 (2023). https://doi.org/10.1140/epjc/s10052-023-11810-6
82. Y. Yan, X. Hu, H. Huang et al., Investigating excited Ω_c states from pentaquark perspective. Phys. Rev. D **108**, 094045 (2023). https://doi.org/10.1103/PhysRevD.108.094045
83. Y. Yan, H. Huang, X. Zhu et al., Prediction of P_{cc} states in a quark model. Phys. Rev. D **109**, 034036 (2024). https://doi.org/10.1103/PhysRevD.109.034036
84. H. Huang, H. Pang, J. Ping, Study of N anti-N interaction with channel-coupling in constituent quark models. Mod. Phys. Lett. A **26**, 1231 (2011). https://doi.org/10.1142/S0217732311035481
85. H. Huang, J. Ping, F. Wang, Study of $p\bar{\Lambda}$ and $p\bar{\Sigma}$ systems in constituent quark models. Mod. Phys. Lett. A **27**, 1250039 (2012). https://doi.org/10.1142/S0217732312500393
86. M. Chen, H. Huang, J. Ping et al., Quark model study of strange dibaryon resonances. Phys. Rev. C **83**, 015202 (2011). https://doi.org/10.1103/PhysRevC.83.015202
87. J. Vijande, F. Fernandez, A. Valcarce, Constituent quark model study of the meson spectra. J. Phys. G **31**, 481 (2005). https://doi.org/10.1088/0954-3899/31/5/017
88. S. Navas et al., [Particle Data Group], Review of particle physics. Phys. Rev. D **110**, 030001 (2024). https://doi.org/10.1103/PhysRevD.110.030001
89. M. Xu, M. Yu, L. Liu, Examining the crossover from hadronic to partonic phase in QCD. Phys. Rev. Lett. **100**, 092301 (2008). https://doi.org/10.1103/PhysRevLett.100.092301
90. S.E. Koonin, Proton pictures of high-energy nuclear collisions. Phys. Lett. B **70**, 43 (1977). https://doi.org/10.1016/0370-2693(77)90340-9

91. S. Pratt, T. Csorgo, J. Zimanyi, Detailed predictions for two pion correlations in ultrarelativistic heavy ion collisions. Phys. Rev. C **42**, 2646 (1990). https://doi.org/10.1103/PhysRevC.42.2646
92. W. Bauer, C.K. Gelbke, S. Pratt, Hadronic interferometry in heavy ion collisions. Ann. Rev. Nucl. Part. Sci. **42**, 77 (1992). https://doi.org/10.1146/annurev.ns.42.120192.000453
93. D. L. Mihaylov, V. Mantovani Sarti, O.W. Arnold et al., A femtoscopic correlation analysis tool using the Schrödinger equation (CATS). Eur. Phys. J. C **78**, 394 (2018). https://doi.org/10.1140/epjc/s10052-018-5859-0
94. K. Chadan and P.C. Sabatier, *Inverse Problems in Quantum Scattering Theory*, 2nd ed. (Springer, Berlin and Heidelberg, 1989). https://doi.org/10.1007/978-3-642-83317-5
95. V.A. Marchenko, On reconstruction of the potential energy from phases of the scattered waves. Dokl. Akad. Nauk SSSR **104**, 695 (1955)
96. Z.S. Agranovich, V.A. Marchenko, *The Inverse Problem of the Scattering Theory* (Gordon and Breach, New York and London, 1963)
97. S.A. Sofianos, A. Papastylianos, H. Fiedeldey et al., Role of Levinson's theorem in neutron deuteron quartet *S* wave scattering. Phys. Rev. C **42**, R506 (1990). https://doi.org/10.1103/PhysRevC.42.R506
98. S.E. Massen, S.A. Sofianos, S.A. Rakityansky et al., Resonances and off-shell characteristics of effective interactions. Nucl. Phys. A **654**, 597 (1999). https://doi.org/10.1016/S0375-9474(99)00316-4
99. R.G. Newton, *Scattering Theory of Waves and Particles*, 2nd ed. (Springer, Berlin and Heidelberg, 1982). https://doi.org/10.1007/978-3-642-88128-2
100. L. Jade, M. Sander, H.V. von Geramb, Modeling of nucleon-nucleon potentials, quantum inversion versus meson exchange pictures. Lect. Notes Phys. **488**, 124 (1997). https://doi.org/10.1007/BFb0104930
101. N.A. Khokhlov, L.I. Studenikina, Energy-independent complex $^0S_1$NN potential from the Marchenko equation. Phys. Rev. C **104**, 014001 (2021). https://doi.org/10.1103/PhysRevC.104.014001
102. N.A. Khokhlov, Energy-independent complex single-*P*-waves *NN* potential from the Marchenko equation. Phys. Rev. C **107**, 044001 (2023). https://doi.org/10.1103/PhysRevC.107.044001
103. J.A. Wheeler, Molecular viewpoints in nuclear structure. Phys. Rev. **52**, 1083 (1937). https://doi.org/10.1103/PhysRev.52.1083
104. M. Kamimura, Chapter V. A coupled channel variational method for microscopic study of reactions between complex nuclei. Prog. Theor. Phys. Suppl. **62**, 236 (1977). https://doi.org/10.1143/PTPS.62.236
105. Y. Yan, Q. Huang, X. Zhu et al., Investigating Ξ resonances from a pentaquark perspective. Phys. Rev. D **110**, 014021 (2024). https://doi.org/10.1103/PhysRevD.110.014021
106. V.A. Babenko, N.M. Petrov, Correlation between the deuteron characteristics and the low-energy triplet np scattering parameters. Phys. Atom. Nucl. **66**, 1319 (2003). https://doi.org/10.1134/1.1592586
107. S. Acharya et al. [ALICE], Search for a common baryon source in high–multiplicity pp collisions at the LHC. Phys. Lett. B **811**, 135849 (2020) [erratum: Phys. Lett. B **861**, 139233 (2025)]. https://doi.org/10.1016/j.physletb.2020.135849
108. S. Acharya et al. [ALICE], Common femtoscopic hadron–emission source in *pp* collisions at the LHC. Eur. Phys. J. C **85**, 198 (2025) [erratum: Eur. Phys. J. C **86**, 12 (2026)]. https://doi.org/10.1140/epjc/s10052-025-13793-y
109. D. Mihaylov and J. González González, Novel model for particle emission in small collision systems. Eur. Phys. J. C **83**, 590 (2023). https://doi.org/10.1140/epjc/s10052-023-11774-7
110. D.F. Wang, M.Y. Chen, Y.G. Ma et al., Investigating the pion emission source in *pp* collisions using the AMPT model with subnucleon structure. Nucl. Sci. Tech. **36**, 154 (2025). https://doi.org/10.1007/s41365-025-01722-3
111. O. Vázquez Doce, D. Mihaylov and L. Fabbietti, Study of the deuterons emission time in *pp* collisions at the LHC via kaon–deuteron correlations. Eur. Phys. J. A **61**, 53 (2025). https://doi.org/10.1140/epja/s10050-025-01534-4
112. P. Braun-Munzinger, B. Dönigus, Loosely-bound objects produced in nuclear collisions at the LHC. Nucl. Phys. A **987**, 144 (2019). https://doi.org/10.1016/j.nuclphysa.2019.02.006
113. J.H. Chen, J. Chen, F.K. Guo et al., Production of exotic hadrons in *pp* and nuclear collisions. Nucl. Sci. Tech. **36**, 55 (2025). https://doi.org/10.1007/s41365-025-01664-w
114. D. Johnson, I. Polyakov, T. Skwarnicki et al., Exotic Hadrons at LHCb. Ann. Rev. Nucl. Part. Sci. **74**, 583 (2024). https://doi.org/10.1146/annurev-nucl-102422-040628
115. T. Shao, J.H. Chen, J. Pochodzalla et al., Measurement of ^{6}H ground state energy in an electron scattering experiment at MAMI-A1. Phys. Rev. Lett. **134**, 162501 (2025). https://doi.org/10.1103/PhysRevLett.134.162501
116. J. Haidenbauer, U.G. Meißner, A. Nogga, Hyperon-nucleon interaction within chiral effective field theory revisited. Eur. Phys. J. A **56**, 91 (2020). https://doi.org/10.1140/epja/s10050-020-00100-4
117. B. Aboona, J. Adam, J.R. Adams et al., Observation of directed flow of hypernuclei ${}^3_\Lambda$H and ${}^4_\Lambda$H in $\sqrt{s_{\rm NN}} = 3$ GeV Au+Au collisions at RHIC. Phys. Rev. Lett. **130**, 212301 (2023). https://doi.org/10.1103/PhysRevLett.130.212301
118. J. Chen, X. Dong, Y.G. Ma et al., Measurements of the lightest hypernucleus (${}^3_\Lambda$H): progress and perspective. Sci. Bull. **68**, 3252 (2023). https://doi.org/10.1016/j.scib.2023.11.045
119. S. Acharya, D. Adamová, A. Adler et al., Measurement of the lifetime and Λ separation energy of ${}^3_\Lambda$H. Phys. Rev. Lett. **131**, 102302 (2023). https://doi.org/10.1103/PhysRevLett.131.102302
120. Y.G. Ma, Hypernuclei as a laboratory to test hyperon-nucleon interactions. Nuc. Sci. Tech. **34**, 97 (2023). https://doi.org/10.1007/s41365-023-01248-6
121. J.H. Chen, L.S. Geng, E. Hiyama et al., Perspectives for hyperon and hypernuclei physics. Chin. Phys. Lett. **42**, 100101 (2025). https://doi.org/10.1088/0256-307X/42/10/100101
122. B.I. Abelev, M. M. Aggarwal, Z. Ahammed et al., STAR, observation of an antimatter hypernucleus. Science **328**, 58 (2010). https://doi.org/10.1126/science.1183980
123. STAR Collaboration, observation of the antimatter hypernucleus ${}^4_{\bar\Lambda}\bar{\rm H}$. Nature **632**, 1026 (2024). https://doi.org/10.1038/s41586-024-07823-0